International Journal of Biological Macromolecules 332 (2025) 148479

Contents lists available at ScienceDirect

International Journal of Biological Macromolecules

journal homepage: www.elsevier.com/locate/ijbiomac

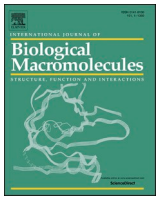

Covalently linked dimers of a G-quadruplex-forming aptamer as HMGB1 inhibitors

Andrea Criscuolo [1], Ettore Napolitano [1], Claudia Riccardi, Rosa Gaglione, Erika Piccolo, Angela Arciello, Domenica Musumeci [*], Daniela Montesarchio [*]

Department of Chemical Sciences, University of Naples Federico II, via Cintia 21, 80126, Napoli, Italy

ARTICLE INFO

Keywords:
Aptamers
HMGB1
G-quadruplex structures
Dimerization
Protein binding and inhibition

ABSTRACT

We here studied a focused set of covalent dimers of the G-quadruplex(G4)-forming aptamer L12, a 26-mer previously selected as inhibitor of High Mobility Group Box 1 (HMGB1), protein involved in various inflammatory and autoimmune diseases as well as in cancer. Inspired by the ability of L12 to form dimeric parallel G4 structures, proved to be highly bioactive towards HMGB1, we investigated several covalent dimeric analogues of L12, whose design exploited linkers of different nature and length, maintaining or inverting the polarity of the two L12 strands in the sequence. Several biophysical techniques were used to analyze the conformational behaviour, molecularity and thermal/serum stability of these dimers, which formed G4 structures of parallel or hybrid topologies. Their ability to interact with the target HMGB1 protein and inhibit HMGB1-induced cellular migration was tested in comparison with L12 non-covalent dimer. The best candidate was L12d1T3, containing a single thymidine as 3′-3′ inversion of polarity motif in the junction between the two L12 strands. This oligonucleotide, forming a parallel G4 structure, showed strong affinity for the target protein (K_D *ca.* 40 nM), marked serum resistance ($t_{1/2}$ *ca.* 13 h), and excellent ability to hamper cell migration in A549 cells, with IC_{50} of 28 nM.

1. Introduction

High mobility group box 1 (HMGB1) is a highly conserved non-histone DNA-binding protein with a pivotal role in a series of crucial cellular functions, including regulation of gene transcription as well as DNA remodelling and repair [1]. This protein is known for its ability to recognize with high affinity distorted or damaged DNA structures, such as four-way junctions, cisplatin-modified DNA duplexes and also G-quadruplexes [2–5]. When released in the extracellular matrix, HMGB1 acts as a cytokine, playing a key role in inflammation and immune responses [6]. Additionally, HMGB1 is involved in the pathogenesis of various diseases, including cancer, neurodegenerative disorders, and inflammatory conditions [7,8]. In cancer, HMGB1 is implicated in several key processes that contribute to tumour onset, progression and metastasis and can also actively promote tumour growth by stimulating angiogenesis through the production of pro-inflammatory cytokines and growth factors [9]. Furthermore, since high levels of HMGB1 were found in sera and tissues of patients with different cancer types, including non-small cell lung cancer (NSCLC) — the most common and aggressive type of lung cancer — HMGB1 was suggested as a powerful diagnostic biomarker to evaluate NSCLC progression and therapy response [10–12], as well as to detect, among others, urothelial bladder carcinoma (UBC), malignant mesothelioma, pancreatic ductal adenocarcinoma (PDAC) and gastric and colorectal carcinomas [13]. For these reasons, targeting HMGB1 and inhibiting its signalling activity may represent not only a therapeutic strategy for cancer and inflammation treatment, but also a potential diagnostic tool for early cancer detection.

In the search for novel, effective inhibitors of HMGB1, we recently identified, by an *in vitro* selection procedure applied to a doped library of guanine-rich oligonucleotides, a set of G-quadruplex(G4)-forming aptamers able to specifically recognize this protein [14]. The selected DNA sequences were studied in PBS, a pseudo-physiological buffer mimicking the extracellular medium, where HMGB1 exerts its pathological activity, using spectroscopic, electrophoretic, and chromatographic techniques. All these aptamers proved to be highly polymorphic, forming monomeric G4s of different topologies and, in some cases, dimeric G4 species. Remarkably, the protein preferentially recognized the sequences forming dimeric parallel G4 structures, which also proved

* Corresponding authors.
E-mail addresses: domenica.musumeci@unina.it (D. Musumeci), daniela.montesarchio@unina.it (D. Montesarchio).
[1] *These authors equally contributed to the work*

https://doi.org/10.1016/j.ijbiomac.2025.148479
Received 3 June 2025; Received in revised form 10 September 2025; Accepted 21 October 2025
Available online 22 October 2025

to be the most effective inhibitors in HMGB1-induced cell migration assays. The aptamer named L12, with sequence 5′-TTAGGGATTGG-GAATGGGTATGGGTT-3′, proved to be particularly promising among the tested oligonucleotides. This G4-forming aptamer, having marked propensity to form dimeric species, showed high thermal and serum stability, no toxicity on healthy cells, along with potent anti-HMGB1 activity (IC_{50} of *ca.* 28 nM) and good binding affinity for the protein (K_D of *ca.* 26 and 104 nM calculated for the separated dimeric and monomeric species, respectively) [14]. In addition, we investigated the same set of aptamers under the same solution conditions after a standard annealing procedure [15], typically introduced to favour the formation of thermodynamically preferred conformations. Remarkably, upon annealing, all the identified anti-HMGB1 aptamers lost their dimeric forms, exclusively forming monomeric G4 structures, featured by poorer thermal and nuclease stabilities, along with lower protein affinity and inhibition efficiency with respect to the dimeric species, obtained from their not-annealed counterparts [15]. The latter results further corroborated our idea of focusing on dimeric G4 structures, which are indeed preferred by the target HMGB1 protein, in analogy with other cancer-related proteins, as *e.g.* $VEGF_{165}$ [16].

Therefore, taking inspiration from recent literature showing that many protein-binding aptamers were significantly optimized by engineering suitable bivalent or multivalent analogues of the original oligonucleotides [17–19], we here report the design and characterization of a set of covalently linked L12 dimers. The conformational behaviour, serum stability and molecularity of these dimers were investigated by using several biophysical techniques, particularly evaluating the influence on aptamer structuring of different selected linkers, able to maintain or invert the polarity of the two L12 strands in the sequence. Moreover, in view of their potential use as HMGB1 inhibitors *in vivo*, the affinity and bioactivity towards HMGB1 as well as the nuclease resistance in serum of these L12 analogues were determined and their overall properties analyzed in comparison with the parent, non-covalent L12 dimeric species.

2. Results and discussion

2.1. Design of the L12 covalent dimers

In the absence of detailed structural data on the species formed by L12, in particular of the dimeric forms present in L12 samples when not previously subjected to annealing (N.A. L12), the design of the covalent dimers was based on the use of linkers of different nature and length, also varying the orientation of the two L12 strands *via* 3′-5′, 3′-3′ or 5′-5′ junctions (Fig. 1).

To obtain a focused library of L12 covalent dimers, different approaches were explored. In one case, by adopting a strategy widely exploited in the construction of dimeric aptamers [17,20–23], we introduced, in the middle of the sequence, thymidine-based linkers containing a different number of nucleotide units, *i.e.* 1, 2, 4 or 7. The selected T-containing linkers connected the 3′-end of one L12 strand with the 5′-end of the other in the covalent dimers indicated as L12d1T, L12d2T, L12d4T and L12d7T (Table 1), thus maintaining the 5′-3′ polarity throughout all the oligonucleotide sequence. In addition, one thymidine unit was used to connect either the 3′ or 5′ termini of two L12 strands, respectively in L12d1T3 and L12d1T5, providing dimeric species with a 3′-3′ or 5′-5′ inversion of polarity in the middle of the sequence (Table 1).

In another case, a triethylene glycol-based linker (hereafter indicated as Spacer 9 or S9), having approximately the same length of a dinucleotide, was introduced in L12dS9 and L12dS95 derivatives (Table 1). Spacer 9 connected the 3′-end of the first L12 strand with the 5′-end of the second one in L12dS9, thus imparting the 5′-3′ polarity along the whole oligonucleotide strand, whereas in L12dS95 it connected the 5′ extremities of two L12 strands, generating a covalent dimer with a 5′-5′ inversion of polarity site. Moreover, in L12dD3 a symmetric doubler, with length similar to a trinucleotide, was used to link the 3′-ends of two L12 strands so to insert a 3′-3′ inversion of polarity site in the middle of the sequence (Table 1). Thus, L12dS9 can be considered an analogue of L12d2T (same linker length and strands orientation) but containing a more flexible linker, whereas L12dS95 (with a 5′-5′ junction) and L12dD3 (with a 3′-3′ junction) can be considered analogues of L12d1T5 and L12d1T3, respectively, having the same strands connection but longer and more flexible linkers.

Lastly, we also included in this study L12dFB, obtained by connecting the first L12 strand, deprived of its 3′ terminal TT block, with an intact, second L12 oligonucleotide maintaining the 5′-3′ orientation, so to have a 50-mer, *i.e.* a shorter covalent L12 dimer, lacking two nucleotides in the middle with respect to two consecutively linked L12 strands and having the general sequence $(XXXGGG)_8TT$ (X = T or A, as indicated in Table 1).

2.2. Biophysical characterization of the covalent L12 dimers

All the covalently linked L12 dimers were analyzed after annealing in PBS (Phosphate-Buffered Saline), a Na^+-rich buffer mimicking the extracellular environment where HMGB1 exerts its cytokine activity. In particular, the conformational behaviour, thermal stability and molecularity of the studied systems were examined by UV and circular dichroism (CD) spectroscopic analyses, as well as size exclusion chromatography (SE-HPLC) and native polyacrylamide gel electrophoresis (PAGE) experiments, using the parent L12 aptamer as reference.

2.2.1. UV spectroscopic analysis

As a first step, thermal difference spectra (TDS) of the studied systems were obtained by subtracting the oligonucleotide UV spectra recorded at 10 °C from the ones obtained at 95 °C (Fig. S1). TDS profiles can be considered as fingerprints of specific DNA secondary structures

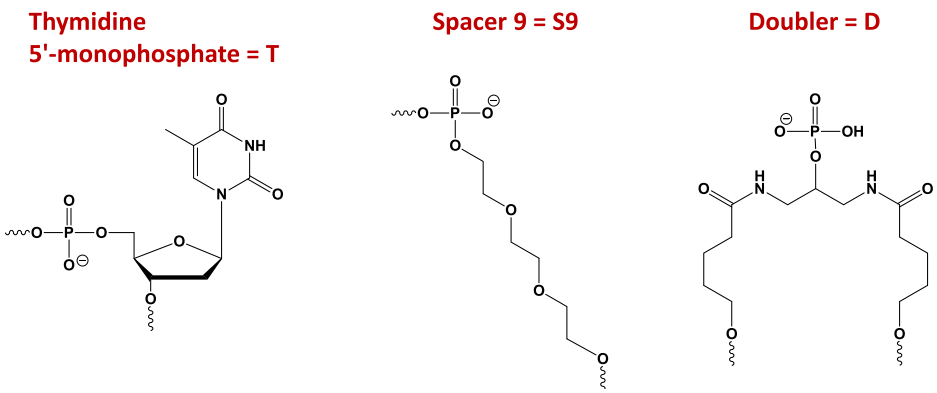

Fig. 1. Molecular structures of the linkers used to obtain the here studied covalently linked L12 dimers.

Table 1
Covalently linked L12 dimers investigated in this study and their features.

Dimer name	Linker type	Strands connection	Sequence	Length
L12d1T	1 T	3′-5′	$^{5'}$TTAGGGATTGGGAATGGGTATGGGTT$^{3'}$**T**$^{5'}$TTAGGGATTGGGAATGGGTATGGGTT$^{3'}$	53-mer
L12d2T	2 T	3′-5′	$^{5'}$TTAGGGATTGGGAATGGGTATGGGTT$^{3'}$**TT**$^{5'}$TTAGGGATTGGGAATGGGTATGGGTT$^{3'}$	54-mer
L12d4T	4 T	3′-5′	$^{5'}$TTAGGGATTGGGAATGGGTATGGGTT$^{3'}$**TTTT**$^{5'}$TTAGGGATTGGGAATGGGTATGGGTT$^{3'}$	56-mer
L12d7T	7 T	3′-5′	$^{5'}$TTAGGGATTGGGAATGGGTATGGGTT$^{3'}$**TTTTTTT**$^{5'}$TTAGGGATTGGGAATGGGTATGGGTT$^{3'}$	59-mer
L12d1T3	1 T	3′-3′	$^{5'}$TTAGGGATTGGGAATGGGTATGGGTT$^{3'}$**T**$^{3'}$TTGGGTATGGGTAAGGGTTAGGGATT$^{5'}$	53-mer
L12d1T5	1 T	5′-5′	$^{3'}$TTGGGTATGGGTAAGGGTTAGGGATT$^{5'}$**T**$^{5'}$TTAGGGATTGGGAATGGGTATGGGTT$^{3'}$	53-mer
L12dS9	S9	3′-5′	$^{5'}$TTAGGGATTGGGAATGGGTATGGGTT$^{3'}$**S9**$^{5'}$TTAGGGATTGGGAATGGGTATGGGTT$^{3'}$	52-mer + S9
L12dS95	S9	5′-5′	$^{3'}$TTGGGTATGGGTAAGGGTTAGGGATT$^{5'}$**S9**$^{5'}$TTAGGGATTGGGAATGGGTATGGGTT$^{3'}$	52-mer + S9
L12dD3	D	3′-3′	$^{5'}$TTAGGGATTGGGAATGGGTATGGGTT$^{3'}$**D**$^{3'}$TTGGGTATGGGTAAGGGTTAGGGATT$^{5'}$	52-mer + D
L12dFB	No linker	3′-5′	$^{5'}$TTAGGGATTGGGAATGGGTATGGGTTAGGGATTGGGAATGGGTATGGGTT$^{3'}$	50-mer

and are particularly useful to identify the presence in solution of G4 structures [24–27]. As expected, all the investigated covalent L12 dimers exhibited a TDS profile typical of a G4 structure (Fig. S1), exhibiting the diagnostic negative band at around 295 nm and positive bands at *ca.* 240 and 275 nm [24–27].

2.2.2. CD spectra and CD-monitored thermal denaturation analysis

To investigate the conformational behaviour and thermal stability of the G-quadruplex structures formed by the covalent L12 dimers, a CD analysis was performed. CD spectra of all the sequences were recorded (Fig. 2, panels a-c) and compared to the ones of the isolated monomeric and dimeric species, as obtained by HPLC purification of N.A. L12 samples (see experimental part), folded respectively in hybrid and parallel G4 structures (Fig. 2, panel d), as previously reported [14,15].

The CD spectra of the covalent L12 dimers were grouped on the basis of their conformational similarity (Fig. 2). Remarkably, all the dimeric constructs which maintained the same orientation (5′-3′) of the two linked L12 strands adopted a hybrid G4 conformation (L12 monomer-like profiles), whereas the oligonucleotides containing a 3′-3′ or 5′-5′ inversion of polarity site in the junction between the two L12 tracts adopted mainly parallel G4 conformations (L12 dimer-like profiles). In turn, L12dFB exhibited a CD profile consistent with the presence of a mixture of G4 structures [28–31].

Singular value decomposition (SVD) analysis [32] allowed determining the percentage of each G4 conformation (parallel, antiparallel, hybrid) (Table S1) that contributed to the different species, thus confirming the attribution of the CD profiles to the various G4 topologies reported above.

Then, by following the CD signal maximum of each oligonucleotide upon increasing the temperature [33] in the 10–95 °C range, CD-monitored melting experiments were carried out. A generally low thermal stability was observed for all the investigated G4 structures (Fig. 3), in most cases even lower than that of monomeric L12, having a T_m value of 36 °C [15]. Interestingly, L12d1T3 and L12d1T5 showed the highest T_m values in the series (40 and 43 °C, respectively), suggesting that the inversion of polarity site containing a short and conformationally constrained linker allowed the formation of G4 structures essentially stable at physiological temperature. In turn, all the covalent dimers with the thymidine-based linker maintaining the same strand polarity along the whole sequence exhibited T_m values of *ca.* 29–30 °C, demonstrating that keeping the same strand polarity in joining two L12 sequences was detrimental for the G4 thermal stability of the aptamer. In

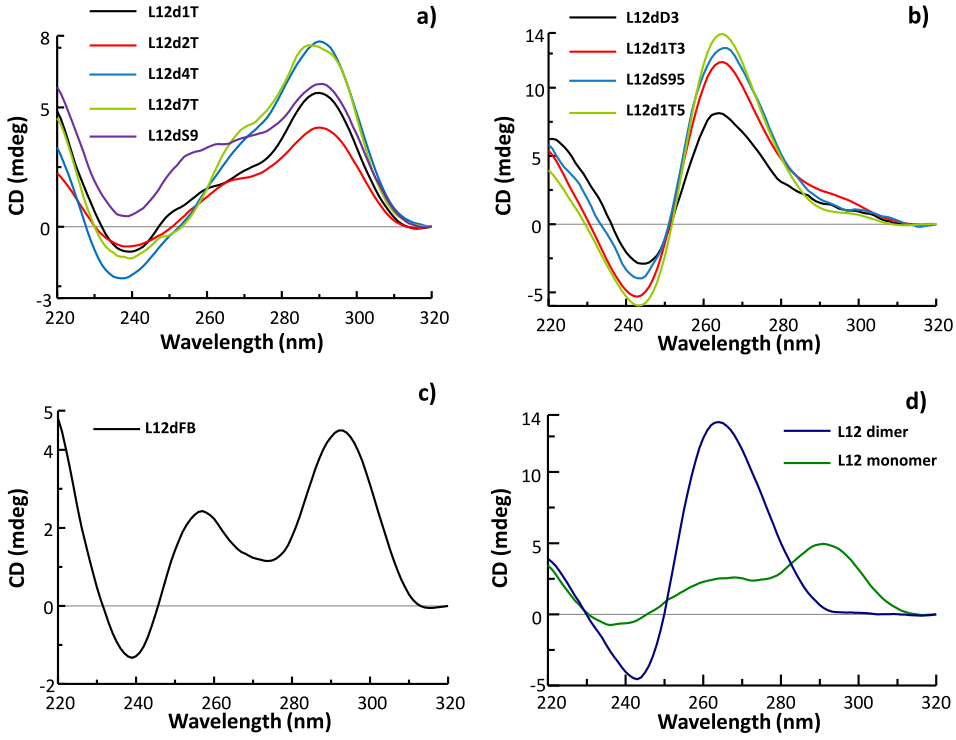

Fig. 2. Representative CD spectra of the covalent L12 dimers, all annealed at 1 μM, grouped by G4 conformational similarity (panel a-c), and of the non-covalent dimeric and monomeric L12 species (panel d), both isolated from N.A. L12 samples (2 μM per single strand). All the CD spectra were recorded at 20 °C in PBS in 1 cm path length cuvette. (For interpretation of the overlapped CD spectra, the reader should refer to the web version of this article.)

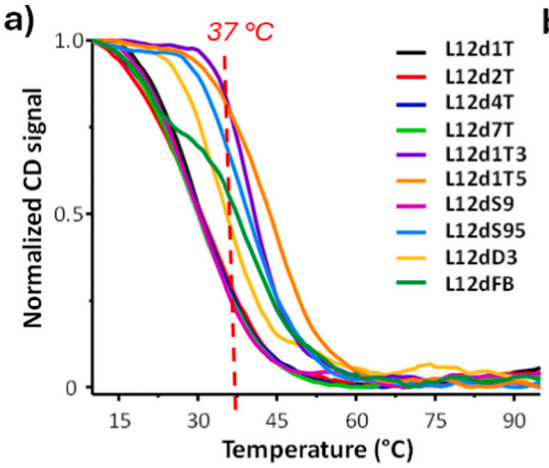

b)

Seq. name	T_m (± 1°C) / λ_{max} (nm)
L12d1T	29 (290)
L12d2T	30 (289)
L12d4T	30 (290)
L12d7T	29 (289)
L12d1T3	40 (265)
L12d1T5	43 (265)
L12dS9	30 (292)
L12dS95	39 (266)
L12dD3	33 (264)
L12dFB	20 - 39 (293)

Fig. 3. a) Representative overlapped CD-melting profiles recorded at the maximum ellipticity observed at 10 °C for each L12 covalent dimer at 1 μM concentration in PBS (1 °C/min scan rate). The normalized CD signals were reported as a function of the temperature (°C). b) Apparent T_m values obtained by elaboration of the CD-melting curves of panel a) at the indicated wavelength. (For interpretation of the overlapped CD-melting curves, the reader should refer to the web version of this article.)

the case of L12dFB, two separate transitions were observed in the thermal denaturation process (Fig. 3a), with apparent T_m values of *ca.* 20 and 39 °C (Fig. 3b), probably due to the coexistence of hybrid/antiparallel G4s of different thermal stability, both contributing to the 293 nm band (Table S1).

Additionally, to better analyze the melting process of the oligonucleotides, CD spectra every 5 °C were recorded, showing a progressive reduction of the main CD band upon heating, with complete denaturation at 95 °C (Fig. S2). The cooling experiments indicated low-to-moderate hysteresis under the experimental conditions tested (Fig. S3 and Table S2), clearly evidencing that all the covalently linked dimers showed almost reversible folding/unfolding processes.

2.2.3. *Evaluation of the molecularity of the L12 covalent dimers*

The molecularity of the L12 covalent dimers was evaluated by size exclusion chromatography (SE-HPLC) [34–36] and native polyacrylamide gel electrophoresis (PAGE) experiments in PBS [37], using N.A. L12, containing both monomeric and dimeric species [14], as a reference. Interestingly, the chromatographic profiles of the covalently linked L12 dimers, analyzed at 2 μM conc., showed essentially a single peak, with a retention time in the range 8.6–9.1 min (Fig. S4). Notably, this peak is comprised between the ones of the monomeric and dimeric species of the parent L12, respectively, demonstrating the formation of monomolecular structures with a generally higher compactness than that of the L12 non-covalent dimeric species. Multiple and broader HPLC peaks were evidenced only for L12dD3 and L12dFB (Fig. S4).

Native PAGE experiments confirmed these findings, showing, for the L12 covalently linked dimers, single bands that migrated faster than the L12 non-covalent dimeric species, which in turn appeared on the gel as multiple bands (probably multiple dimeric structures and/or higher-order structures) [14], slightly slower than the shorter oligonucleotide tel_{46}, a 46-mer [38,39] used as reference for a dimeric G4 species (Fig. S5).

2.3. *HMGB1-binding experiments: Biolayer Interferometry*

Subsequently, the ability of the L12 covalent dimers to interact with the target HMGB1 protein was evaluated by Biolayer Interferometry (BLI) analysis [40], using the parent L12 aptamer as reference. The covalent dimers, equipped with a 5′-biotin tag, were fixed on streptavidin-coated sensors at 50 nM concentration after annealing in PBS. As a reference, we used the non-covalent dimeric species of the 5′-biotinylated analogue of L12, previously isolated from the corresponding N. A. L12 sample by analytical SE-HPLC (see experimental part) and then anchored to the sensors using the same experimental conditions exploited for the covalent dimers. Afterwards, different HMGB1 concentrations were used with each sensor for an association and dissociation time of 3 and 5 min, respectively, along with blank samples containing only the binding buffer as a reference. A global curve fitting of the binding data was performed employing different models, with the 2:1 heterogeneous ligand model affording the best fit (Fig. S6). This model, suitable for processes featured by two independent binding events [41], can be applied in our case considering the two DNA-binding domains on HMGB1, *i.e.* box A and box B of the protein, which can interact with each aptamer with different affinities. The corresponding K_D and K_{D2} values are reported in Table 2. Considering the main binding event, the covalent dimers L12d1 T and L12d2 T, containing one or two thymidines in their linkers, respectively, showed very similar affinity for HMGB1, only slightly lower than that of L12 non-covalent dimeric species (K_D of 61 and 64 nM, respectively, *vs.* 50 nM for the L12 non-covalent dimer). In contrast, the dimers having longer linkers, with 4 or 7 T in the junction between the two L12 strands, had lower affinity for the target protein (K_D of 71 and 90 nM for L12d4T and L12d7T, respectively). This result suggested that, with long linkers, each L12 tract of these dimeric constructs formed an independent G4 structure which could interact with the target protein as a separate entity. This behaviour was also found for the set of dimers containing non-nucleoside linkers and confirmed the above hypothesis, since the highest K_D value of the series was observed for L12dD3, indeed having the longest connecting linker here investigated.

On the other hand, the best binding affinities were obtained for the

Table 2
K_D and K_{D2} values obtained by BLI analysis with their corresponding errors. In all the BLI assays, an $R^2 = 0.99$ was obtained.

	K_D (nM)	K_{D2} (nM)
L12d1T	61 ± 3	300 ± 27
L12d2T	64 ± 2	282 ± 35
L12d4T	71 ± 15	296 ± 50
L12d7T	90 ± 14	208 ± 33
L12d1T3	44 ± 5	424 ± 54
L12d1T5	56 ± 5	201 ± 65
L12dS9	91 ± 2	565 ± 62
L12dS95	76 ± 9	269 ± 28
L12dD3	123 ± 2	407 ± 71
L12dFB	104 ± 12	340 ± 50
L12 dimer	50 ± 9	113 ± 45

dimers with inversion of polarity sites L12d1T3 and L12d1T5, which showed K_D values of 44 and 56 nM, respectively, comparable with that of the L12 non-covalent dimer. These aptamers highlighted a superior affinity for HMGB1 also compared to L12dD3 and L12dS95 (K_D values of 123 and 76 nM, respectively), *i.e.* the L12 covalently linked dimers containing an inversion of polarity site, but with longer and more flexible linkers. Even L12dFB, having the characteristic deletion of the couple of nucleotides TT in the connection site of the linked L12 units, thus allowing 8 continuous repeats of the XXXGGG tract, did not show any improvement in protein affinity.

Altogether, these results indicated that the best L12 covalently linked dimers in terms of HMGB1-binding affinity were the ones having the two L12 sequences connected by a short linker, better if of nucleoside type, and even better if containing a 3′-3′ or 5′-5′ inversion of polarity site.

2.4. Evaluation of the anti-HMGB1 activity by in vitro cellular migration assays

To evaluate the *in vitro* bioactivity of the L12 covalent dimers, we assessed their ability to inhibit the HMGB1-induced cell migration. In pathological conditions, HMGB1 is overexpressed by specific cells (inflammation-related or cancer cells) and released in the extracellular milieu, where it can act as a potent chemotactic agent. In this frame, targeting extracellular HMGB1 is considered a valuable strategy to inhibit cellular migration and invasion. Therefore, we focused on neutralizing extracellular HMGB1 using high-affinity G-quadruplex-forming aptamers. To this aim, we used the human non-small cell lung cancer A549 cell line, naturally expressing and releasing high levels of HMGB1 and for which a key role of the protein in the regulation of cell migration and proliferation was unambiguously determined [42]. For

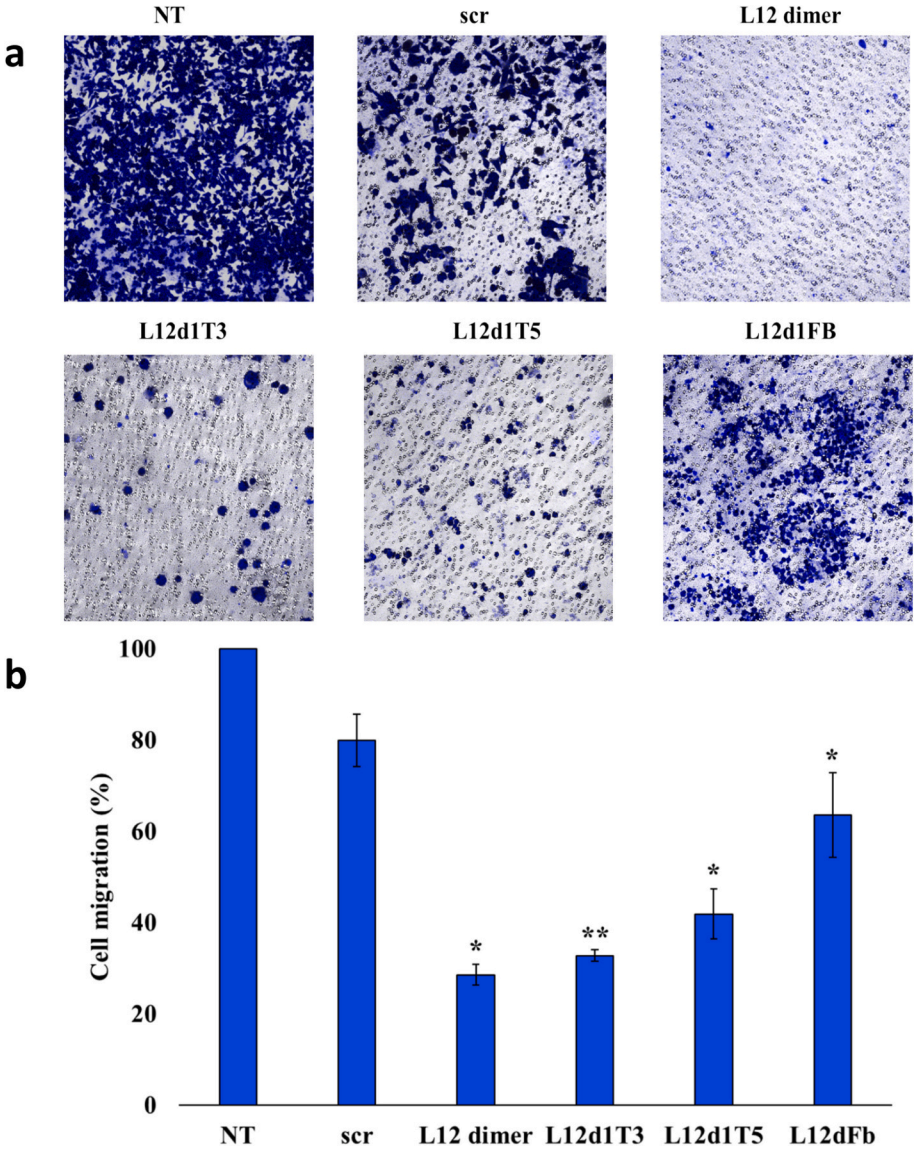

Fig. 4. Chemotaxis assay on human A549 lung cancer cells. Cells were either left untreated (NT) or treated for 24 h with 100 nM L12d1T3, L12d1T5, L12dFb, as well as with the non-covalent L12 dimer, or a scrambled oligonucleotide (scr), used as positive and negative controls, respectively. Cell migration was then assessed over 24 h using 10 % FBS as a chemoattractant. After incubation, cells that had migrated to the lower side of the membrane were fixed, stained with Crystal Violet and photographed under a phase-contrast microscope at 10× magnification. Representative images for each condition (a) were selected from a set of at least eight pictures collected for each of three independent experiments. The histogram (b), based on the average absorbance of the eluted Crystal Violet, quantifies cell migration as a percentage relative to the NT group. The absorbance values, referred to NT cells samples incubated in the absence of FBS, was subtracted from all conditions to correct for basal migration. Data are presented as mean ± SD. Statistical significance was determined using Student's *t*-test; significant differences compared to NT are indicated as follows: $P < 0.05$; $P < 0.01$.

these experiments, we selected two high affinity aptamers (L12d1T3 and L12d1T5) and one with low affinity (L12dFB), all featured by good G4 thermal stability at physiological temperature. A scrambled 26-mer oligonucleotide, containing the same number of guanines as L12 but unable to fold into a G4 structure, here named scr, along with the parent L12 non-covalent dimer [14] were used as negative and positive controls, respectively. The assays were carried out on A549 cells at 37 °C in 24-well plates equipped with 8.0 μm PET translucent inserts *via* simple incubation of the selected oligonucleotides, each provided at 100 nM concentration for 24 h, without addition of transfection reagents, following previously reported protocols [14,43,44]. The cell ability to migrate through the microporous membrane of the upper chambers was evaluated in the presence of 10 % Fetal Bovine Serum (FBS) used as chemo-attractant in the lower compartment and compared to untreated cells (NT), whose migration was set as 100 %. The results showed that the most effective covalently linked L12 dimeric aptamer in inhibiting HMGB1-induced cell migration was L12d1T3, showing an inhibitory activity very similar to that of the parent L12 non-covalent dimer. Notably, a clear correlation between the inhibitory activity towards the protein (Fig. 4) and the HMGB1 binding affinity (Table 2) was found for all the investigated aptamers.

2.5. HMGB1 CD-binding assay

The L12 dimeric analogues L12d1T3 and L12d1T5, with a 3′-3′ and 5′-5′ inversion of polarity site, respectively, proved to be the aptamers with the highest HMGB1 binding affinity and inhibition capability in the explored series. Thus, they were further investigated in their interaction with HMGB1 by using CD-monitored binding experiments, including L12d1T — the dimer with the same nucleoside type linker used in L12d1T3 and L12d1T5, but without inversion of polarity — and L12 non-covalent dimer as controls. For this assay, a two-chamber cuvette, characterized by two distinct compartments, was used. This cuvette allows recording the *sum* and *mix* spectra of two components, *i.e.* the spectra obtained by keeping the oligonucleotide and the protein as separate systems (*sum*, black lines, Fig. 5), and the ones obtained after mixing the two solutions (*mix*, red lines, Fig. 5). First, the CD spectrum of the sole HMGB1 was recorded before each CD *sum* spectrum, confirming the correct folding of the protein in PBS (Fig. S7). Then, each oligonucleotide was added in the neighbour compartment of the same cuvette, allowing the recording of the CD *sum* spectrum of each oligonucleotide and, successively, after turning upside down the cuvette, the CD *mix* one. In case the two analyzed systems do not interact, the *sum* spectrum is essentially superimposable to the *mix* one. In turn, if the two systems do interact, *e.g.* by forming a non-covalent complex, the spectrum obtained after mixing the two solutions differs from the *sum* spectrum. Here, for all the tested sequences, marked differences between the *sum* and *mix* spectra were observed, fully confirming the interaction between the oligonucleotides and HMGB1 (Fig. 5). In detail, for L12d1T3, L12d1T5 and L12d1T, major differences were observed in the 200–250 nm region, while no changes were detected in the 250–300 nm region (Fig. 5), where only DNA contributes to the CD signal (Fig. S7). This behaviour was in agreement with other HMGB1-DNA complexes described in the literature [15,45] and suggested that, upon binding, only the protein underwent significant conformational changes. Interestingly, for L12 non-covalent dimer, significant changes were detected not only in the 200–250 nm region but also in the 250–300 nm region, suggesting that, upon binding, a slight re-modelling of both the protein and the oligonucleotide occurred, probably due to the higher plasticity of this aptamer, formed by multiple non-covalent dimeric G4 conformations (*cfr.* Fig. S5), compared to its covalently linked analogues.

For all the investigated *mix* solutions, CD-monitored melting experiments were also performed by following the maximum CD signal of each system upon gradually increasing the temperature in the 10–95 °C range. In all cases, no stabilizing/destabilizing effects on the G4 structures formed by these oligonucleotides were observed as a result of protein binding (data not shown).

2.6. Evaluation of the serum resistance

In view of their potential use *in vivo* as candidate drugs, the nuclease resistance in serum of L12d1T3 and L12d1T5, shown to be the best

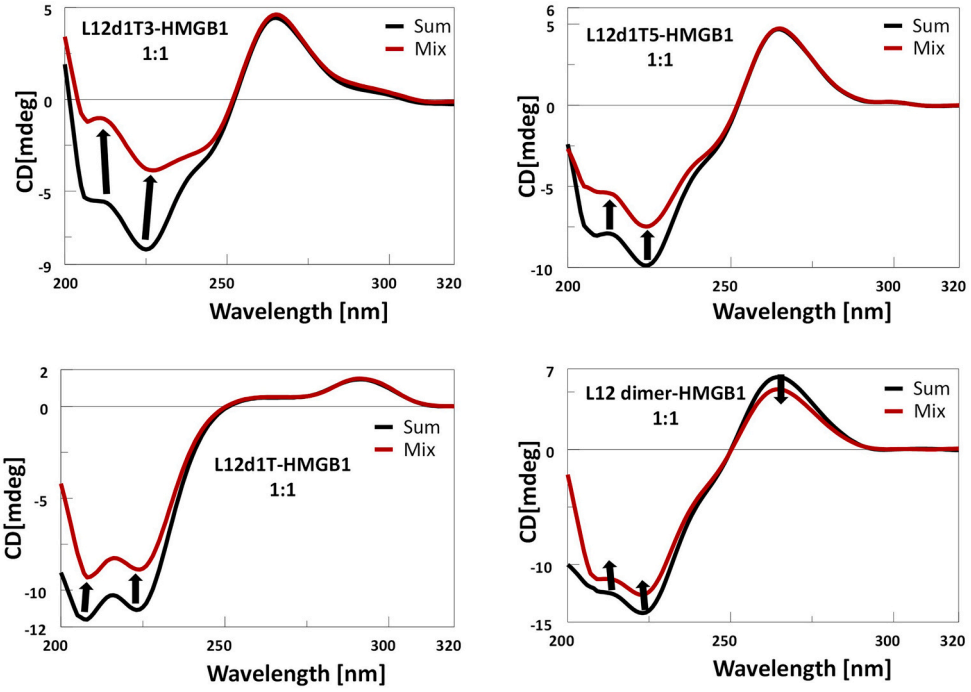

Fig. 5. Representative overlapped *sum* and *mix* spectra relative to the CD-binding experiments between HMGB1 (1 μM) and L12d1T3, L12d1T5 and L12d1T, as well as for L12 non-covalent dimer at 1:1 protein/DNA ratio in PBS. Arrows indicate the changes in the CD spectra after mixing the protein and DNA solutions. (For interpretation of the overlapped *sum* and *mix* CD spectra, the reader should refer to the web version of this article.)

aptamers here investigated, was evaluated along with suitable controls. We exploited a well-consolidated protocol in which each oligonucleotide, after annealing in PBS, was incubated in 80 % FBS at 37 °C, and aliquots of these mixtures were withdrawn at different time points and then loaded on a denaturing polyacrylamide gel [46]. The dimeric constructs having nucleoside linkers with 5′-3′ polarity (*i.e.* L12d1T, L12d2T, L12d4T, L12d7T and L12dFB), here used as negative controls, evidenced very low nuclease stability, showing half-life time values ($t_{1/2}$) ranging between 13 and 40 min (Figs. S8-S10). This very low serum stability could be explained considering their very low apparent T_m values (Fig. 3b), which indicated that their G-quadruplex structures were to a large extent unfolded at physiological temperature. Among the selected dimers containing the inversion of polarity site in the middle of the sequence, L12d1T5, carrying a 5′-5′ junction and two 3′ extremities exposed to the medium, showed a very low nuclease resistance ($t_{1/2}$ of 19 min). Remarkably, L12d1T3, with a 3′-3′ junction and two free 5′-ends, in turn proved to be very resistant to nuclease degradation ($t_{1/2}$ of 13 h, Figs. 6a and S9).

The much higher stability of L12d1T3 compared to L12d1T5 towards nuclease degradation could in part be expected, taking into account that the first aptamer is devoid of free 3′-OH groups, easily attacked by 3′-exonucleases, which are much more abundant than 5′-exonucleases in serum. However, it could also suggest that when the 3′-ends of the two L12 sequences are linked together in L12d1T3, the resulting oligonucleotide folds into a very compact G4 conformation that is much better protected than L12d1T5 to both *exo*- and endonucleases. Indeed, inspection of the uncropped gels of the nuclease degradation experiments of L12d1T3 and L12d1T5 (Figs. 6b and S10) indicated that, along with the progressive degradation of the main band of each covalent dimer, also faster migrating bands were present. In detail, for L12d1T3, the new band, which however never became the predominant one, could be attributed to a species obtained after the cleavage of a few terminal nucleotides at its 5′-ends, migrating quite similarly to the intact oligonucleotide band. In contrast, in the case of L12d1T5, the nuclease degradation produced a band which became predominant after 7 h incubation, with an electrophoretic mobility comparable to the monomeric L12 species (*cfr.* the gel reported in Fig. S11 where the L12 monomer was used as control), suggesting that the enzymatic cleavage mainly occurred at the level of the internal linker, probably more exposed to the medium and thus also to endonucleases degradation.

2.7. Determination of the IC_{50} value of L12d1T3 for inhibiting HMGB1-promoted cell migration

Since the covalent dimer L12d1T3 gave the best results in terms of thermal stability and serum resistance, as well as affinity and activity towards HMGB1, dose-response cell migration experiments were carried out on this aptamer. In detail, A549 cells were allowed migrating alone or in the presence of increasing amounts of L12d1T3 (from 12.5 to 200 nM). A concentration-dependent inhibition of cell migration was observed (Fig. 7), with an IC_{50} value of *ca.* 28 nM. This value is very encouraging considering that it is equal to the one previously found on

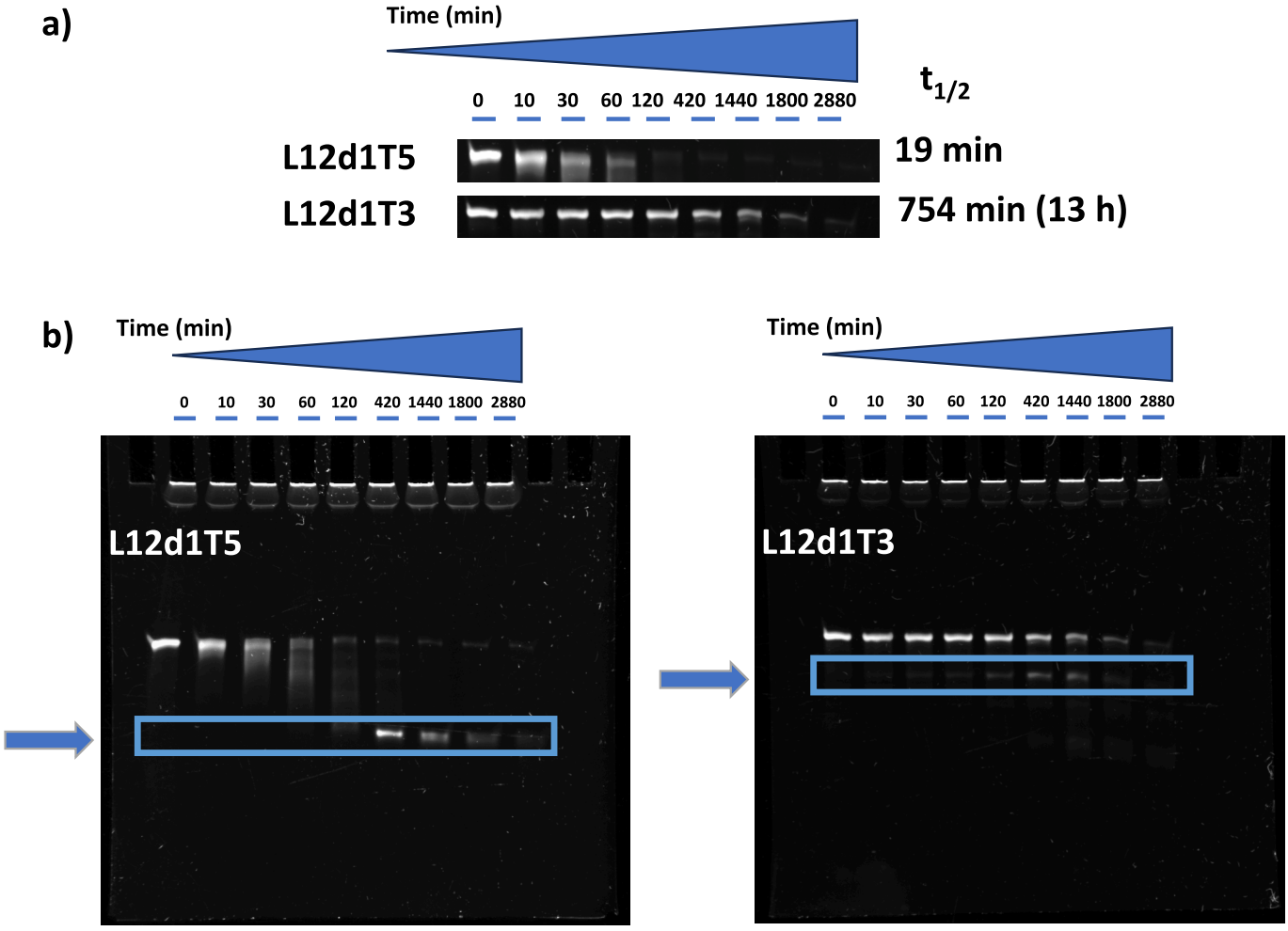

Fig. 6. a) Representative 20 % denaturing PAGE experiments relative to the enzymatic resistance of L12d1T5 and L12d1T3 incubated in 80 % FBS at 37 °C. Aliquots of the reaction mixtures were withdrawn at the indicated time points and loaded on the gel at 1.2 μM concentration. b) Full-size gels of L12d1T5 and L12d1T3 with the rectangles highlighted by the arrows which evidenced the new smaller species formed during the dimer degradation.

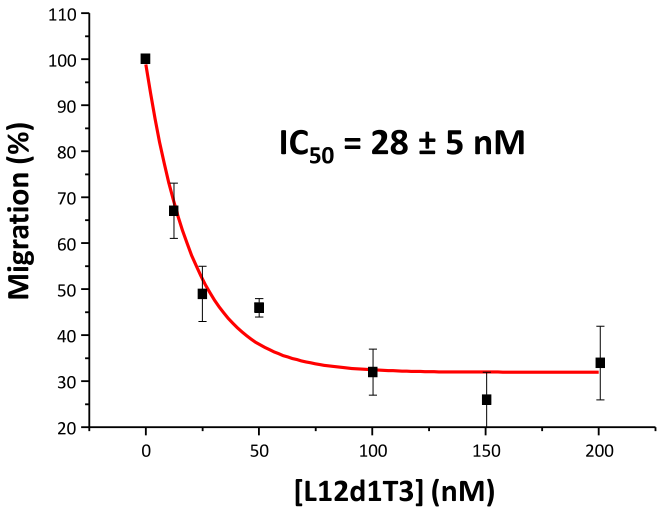

Fig. 7. Chemotaxis assays on human lung cancer A549 cells treated with increasing amounts of L12d1T3. Cells were allowed migrating with increasing concentration of the dimeric aptamer (12.5–200 nM conc. range). Migration is expressed as % with respect to the positive control (not-treated cells). Error bars indicate SD values. Each measurement refers to three independent experiments, each of them consisting of at least two internal replicates. The squares in the graph represent the experimental data and the curve is the best fit obtained (see experimental section for details).

NIH3T3 cells for the parent L12 oligonucleotide as not-annealed sample (*i.e.,* containing both monomeric and dimeric species) [14], and largely better, with a difference of one order of magnitude, than that reported for glycyrrhizin (50 μM), a well-known HMGB1 inhibitor [47].

3. Conclusions

Inspired by the ability of the aptamer L12 to spontaneously fold into dimeric G-quadruplex structures able to act as potent inhibitors of HMGB1 — a protein involved in the pathogenesis of a plethora of inflammatory diseases, as well as of cancer — we here investigated covalently linked dimers of L12, with the aim of obtaining anti-HMGB1 aptamers with improved properties as potential tools for therapeutic and diagnostic applications. In detail, a set of ten covalent L12 dimers, differing for the nature and length of the linker, as well as for the orientation of the connected L12 strands, were herein designed and in-depth characterized in pseudo-physiological conditions. We proved that the dimers which maintained the same orientation (5′ → 3′) of the two connected L12 tracts mainly adopted hybrid G4 conformations, analogously to the parent L12 monomeric species, showing overall poor features, even if to a different extent. Furthermore, longer linkers connecting the two L12 sequences led to a decreased protein recognition, probably because, in these conditions, the two L12 tracts did not interact with each other, binding to the target protein as separated entities. On the other hand, the dimers with an inversion of polarity site, *i.e.* a 3′-3′ or 5′-5′ connection between the two L12 tracts, adopted essentially parallel G4 conformations, analogously to the parent L12 non-covalent dimeric species. In addition, the covalent dimers having an inversion of polarity site characterized by a short and conformationally constrained linker (L12d1T3 and L12d1T5) proved to be better performing aptamers in terms of G4 thermal stability, as well as HMGB1 recognition and inhibition, compared to those having longer and more flexible linkers (L12dS95 and L12dD3). Remarkably, L12d1T3, characterized by a 3′-3′ connection and a single thymidine-based linker in the middle of the sequence, was the best dimeric aptamer of the series showing the highest resistance to nuclease degradation ($t_{1/2}$ = 13 h), very good affinity for the target protein (K_D value of *ca.* 40 nM) and marked ability to inhibit HMGB1-induced cell migration (IC_{50} value of *ca.* 28 nM) — the key event responsible for metastasis — on non-small cell lung cancer A549 cells. L12d1T3 proved to be overall highly superior to the spontaneously formed non-covalent L12 dimer in terms of conformational homogeneity and folding reproducibility. It functions as a valuable ready-to-use, unimolecular system, with reversible folding/unfolding behaviour and marked bioactivity. Indeed, unlike the non-covalent L12 dimer, which forms a mixture of parallel G4 conformations which are not fully reformed after annealing, L12d1T3, upon a standard annealing procedure in PBS, directly folds into a single, well-defined species which is the most bioactive one, having high affinity for the target protein and guaranteeing very reproducible results. This ensures higher consistency, eliminating the need of the purification steps required for the separation of the monomeric and non-covalent dimeric species of L12, and fully supports the progress of L12d1T3 to preclinical studies.

These results are of great value for the development of candidate drugs and diagnostic tools for HMGB1-related pathologies, like cancer. An aptameric drug with the potential to inhibit metastasis in lung cancer or other types of cancer would be game-changing, drastically increasing the survival rate of these very common diseases.

4. Experimental part

4.1. Sample preparation

The set of oligonucleotides reported in Table 1, along with L12, scr (AAGTGTGTGTGTGTGTGTGTGAAG) and tel_{46} [$AGGG(TTAGGG)_7$] reference sequences, with and without biotin tag, were purchased from Biomers.net GmbH (Germany) as HPLC-purified and desalted DNA oligomers in lyophilized form. Each oligonucleotide was dissolved in a defined volume of Ultra-pure nuclease-free water (VWR, Milan, Italy). Their concentration was determined using a UV–Vis/NIR Jasco V-770 spectrophotometer equipped with a Peltier Thermostat JASCO ETCS-761 recording the absorbance at 260 nm and 95 °C in a 1 cm path length quartz cuvette (1 mL internal volume, Hellma). Molar extinction coefficients for the DNA sequences were derived using the Oligo Calculator program, assuming the full unfolding of the oligonucleotides at 95 °C (https://mcb.berkeley.edu/labs/krantz/tools/oligocalc.html) [48]. The oligonucleotide samples were prepared by diluting the initial stock solutions dissolved in water with PBS (PBS: 137 mM NaCl, 2.7 mM KCl, 10 mM NaH_2PO_4/Na_2HPO_4, 1.8 mM KH_2PO_4/K_2HPO_4, pH = 7.3). The diluted solutions were then subjected to an annealing procedure by treating them at 95 °C for 5 min and then allowing them to gradually reach room temperature (r.t.) over 3 h. The samples were finally kept at 4 °C overnight and then taken to r.t. before their use. The reference L12 sequence was subjected or not to the annealing procedure, as indicated in the text, or purified by HPLC providing the dimeric and monomeric isolated species.

4.2. UV spectroscopy analysis

UV spectra for Thermal Difference Spectra (TDS) analysis were recorded with a UV–Vis/NIR Jasco V-770 spectrophotometer equipped with a Peltier Thermostat JASCO ETCS-761 in 1 cm path length quartz cuvettes (1 mL internal volume, Hellma) using the following parameters: 220–320 nm spectral window, medium response, 100 nm/min scanning speed and a 2.0 nm bandwidth. Baseline subtraction was applied appropriately. The investigated oligonucleotides were dissolved in PBS at a concentration of 1 μM. TDS data were obtained by subtracting the UV spectra recorded at 10 °C from those obtained at 95 °C. Each experiment was performed in duplicate. The acquired TDS profiles were then normalized setting to 1 the maximum of absorbance of the difference spectra [24].

4.3. CD spectroscopy analysis

CD spectra and CD-monitored melting/cooling curves were recorded

using a Jasco J-1500 spectropolarimeter equipped with a Jasco CTU-100 circulating thermostat unit in 1 cm path length quartz cuvette (3.5 mL internal volume, Hellma). 1 or 2 μM oligonucleotide solutions in PBS were analyzed at 20 °C using the following parameters: 220–320 nm spectral window, 1 nm data pitch, 2 nm bandwidth, 1 s time response, 100 nm/min scanning speed. All the spectra were averaged over 3 scans and subtracted of the buffer scan [30].

The obtained spectra were processed by using the singular value decomposition (SVD) analysis using the software developed by del Villar-Guerra et al. [32] and converting raw data as previously described [49].

CD-melting/cooling curves were recorded by plotting the CD signal at the maximum ellipticity for each oligonucleotide against the temperature (scan rate of 1 °C/min) within the 10–95 °C range and recording the CD spectra from 220 to 320 nm in 5 °C steps. T_m values were determined as the minima and maxima of the first derivative plots of the melting and cooling curves, with an associated error of ±1 °C. Each experiment was performed in duplicate.

The CD-binding experiments with HMGB1 (HMGBiotech, Milan, Italy) were performed in a two-chamber quartz cell (Hellma, 2 × 0.44 cm optical path length and 2 × 1 mL internal volume), in analogy with previous reports [15,50]. The spectra were recorded in the 200–320 nm range at 20 °C with 5 accumulations, 100 nm/min scanning speed, 1 s response time and 2.0 nm bandwidth. CD spectra were acquired by placing 0.5 mL of 1 μM solutions in PBS of both the oligonucleotide and protein, taken in the two separate compartments of the cell. First, the *sum* spectra of the two separated components were recorded. Then, the cuvette was turned upside down, allowing the solutions of the two components to mix and form a homogeneous solution distributed in the two parts of the cell, and the *mix* spectra were recorded.

4.4. SE-HPLC analysis

SE-HPLC experiments were performed following previously described procedures [14] on an Agilent HPLC system with a UV/vis detector. A Yarra 3 μm analytical column (300 × 4.60 mm; Phenomenex) was used, by monitoring the injected samples at λ = 254 nm and eluting with PBS (pH = 6.9) as mobile phase under a flow rate of 0.35 mL min^{-1}. Injections of 2 μM solutions of each aptamer were performed. Each experiment was repeated twice. For the separation of the monomeric and dimeric species of N.A. L12 as such or with a biotin tag at the 5′-end, a 20 μM solution of the aptamer was used, and the concentration of the two species separated by HPLC was determined by UV analysis as above reported.

4.5. Native PAGE analysis

A 40 % solution of acrylamide/bis-acrylamide (19:1), glycerol, and GelGreen Nucleic Acid Stain were acquired from VWR. Ammonium persulfate (APS) and tetramethylethylenediamine (TEMED) were obtained from Sigma Aldrich.

Oligonucleotide samples in PBS were prepared at a final concentration of 2 μM and loaded onto 20 % polyacrylamide gels with TBE 1× as running buffer (containing 150 mM NaCl and 5 mM KCl). Before loading, all samples were supplemented with 5 % glycerol. The gels were run under native conditions at constant 80 V at r.t. for 3 h. The gels were then stained with GelGreen (supplemented with 0.1 M NaCl) for 30 min and visualized using a UV transilluminator (BioRad ChemiDoc XRS, Milan, Italy). Each experiment was performed in triplicate.

4.6. Biolayer Interferometry kinetic experiments

Binding affinity between HMGB1 and the selected L12 covalent dimers was evaluated by BLI analysis using an Octet R2 system (Sartorius). All steps were performed at 22 °C with shaking at 1000 rpm in a 96-well plate containing 200 μL of different samples in binding buffer [PBS, BSA (0.1 %, *w/v*), Tween-20 (0.02 %, *v*/v), pH 7.4] in each well. A regeneration buffer (Binding buffer containing 0.001 % SDS) was used in the wells dedicated to the regeneration steps. The biotinylated oligonucleotides were immobilized at 50 nM concentration on the streptavidin-coated sensors (Octet SA Biosensors, Sartorius). The functionalized sensors were prepared by using the following steps: baseline (1 min); aptamer loading (2 min); baseline2 (3 min); regeneration (5 s for three times), baseline2 (3 min). Then, various concentrations of HMGB1 protein were added into different wells and analyzed for an association time of 3 min and a dissociation time of 5 min. In detail, 20.4, 40.8, 81.5 and 163 nM HMGB1 concentrations were used for the dimers L12d1T3, L12d1T5, L12d1T, L12d2T, L12d4T and L12d7T; 40.8, 81.5, 163 and 326 nM protein concentrations were used for L12 non-covalent dimer. The protein solutions and blank samples containing only binding buffer as reference were simultaneously analyzed by two functionalized sensors. The sensorgrams obtained from the HMGB1-aptasensor binding were normalized by subtracting the signal simultaneously acquired from the reference functionalized sensors to remove the buffer-induced interferometry shift contribution using Octet Analysis Studio Version 13.0.3.52. Affinity parameters (K_D and K_{D2}) were obtained by using the 2:1 heterogeneous ligand fitting model. The experiments were performed in duplicate. The data are reported as the average values ± SD.

4.7. Serum stability assays

50 μM oligonucleotide solutions in PBS were annealed and then incubated in 80 % FBS (provided by Euroclone, Milan, Italy) at 37 °C for 24 or 48 h (10 μM final concentration). At fixed times, 3 μL of the samples (corresponding to 30 pmol) were collected, mixed with formamide (1:2, *v*/v) to immediately stop the enzymatic degradation, heated at 95 °C for 2 min, and stored at −20 °C until analysis. Then, 4 μL of these solutions (corresponding to 12 pmol), diluted with formamide to a final concentration of 1.2 μM, were supplemented with 5 % glycerol immediately before loading and analyzed by gel electrophoresis on 20 % denaturing PAGE using 8 M urea (VWR, Milan, Italy) in TBE 1× as running buffer. The gels were run at r.t., at constant 200 V for 3 h, then stained with GelGreen (supplemented with 0.1 M NaCl) for 30 min, according to the manufacturer's instructions, and finally visualized using a UV transilluminator (BioRad ChemiDoc XRS, Milan, Italy). Each experiment was performed in triplicate. Then, for each gel, the intensity of DNA bands, at each collected time, was quantified using the FiJi software and normalized with respect to the oligonucleotide treated at time zero, thus allowing the determination of the half-life time values of each oligonucleotide, as previously described [51].

4.8. In vitro migration assays

For the chemotaxis assays, 24-well plates (cellQART) and 8.0 μm PET 24-well translucent inserts (cellQART) were used. A549 cells (adenocarcinomic human alveolar basal epithelial cells) were obtained from ATCC (American Type Culture Collection). DMEM (Dulbecco's Modified Eagle Medium) and Crystal Violet were purchased from Merck, Milan, Italy. A549 cells were cultured in DMEM medium supplemented with 1 % penicillin/streptomycin solution (Sigma-Aldrich) and 10 % FBS (Sigma-Aldrich). Then they were seeded in serum-free DMEM in 12-well plates (70,000 cells/well) and pretreated for 24 h with 100 nM of L12d1T3, L12d1T5, L12dS95 and L12dFB, along with scr and L12 non-covalent dimer used as controls, or left untreated. After 24 h, cells were detached, washed in serum-free DMEM, counted and 70,000 cells/well (in 0.1 mL) were resuspended in serum-free DMEM containing 100 nM of L12d1T3, L12d1T5, L12dS95, L12dFB, scr and L12 non-covalent dimer or serum-free DMEM alone (untreated point). Cells were then added in the transwell insert (upper chamber), whereas the lower chamber was filled with 600 μL DMEM containing 10 % FBS, allowing cell migration for additional 24 h. Untreated cells (NT) in the upper chamber were coupled to both FBS or less-FBS in the lower chamber so

to have, respectively, the highest (100 %) or basal (*ca.* 17 %) migration. Then, the migrated cells were stained with 0.1 % Crystal Violet in 25 % methanol and representative images were acquired using a phase-contrast microscope at 10× magnification. Crystal Violet was then eluted with 1 % SDS and quantified at a microplate reader (ThermoFisher Scientific, Waltham, MA, USA) by measuring the absorbance at 590 nm. The assay was repeated twice affording substantially identical results. All the data represent the mean ± SEM of duplicate measurements.

A similar assay was performed to determine the IC_{50} value of L12d1T3. A549 cells were pretreated for 24 h with L12d1T3 at 12.5–25–50-100-150-200 nM concentrations. After 24 h, cells were washed in serum-free DMEM and 70,000 cells/well (in 0.1 mL) were resuspended in serum-free DMEM containing the selected concentrations of L12d1T3 and seeded in the transwell upper chambers. Then, the assay was performed as described above. The IC_{50} value was calculated by fitting the data with the following decay equation: $y = a * e^{-x/t} + b$, where a is the initial amplitude of the decay, t is the decay constant and b is the asymptotic value. Origin 8.0 was used to perform the fitting.

CRediT authorship contribution statement

Andrea Criscuolo: Writing – review & editing, Writing – original draft, Methodology, Investigation, Data curation, Conceptualization. **Ettore Napolitano:** Writing – review & editing, Writing – original draft, Methodology, Investigation, Data curation, Conceptualization. **Claudia Riccardi:** Writing – review & editing, Writing – original draft, Methodology, Data curation, Conceptualization. **Rosa Gaglione:** Writing – review & editing, Writing – original draft, Methodology, Investigation, Data curation. **Erika Piccolo:** Writing – review & editing, Writing – original draft, Methodology, Investigation, Data curation. **Angela Arciello:** Writing – review & editing, Writing – original draft, Resources, Methodology, Data curation. **Domenica Musumeci:** Writing – review & editing, Writing – original draft, Resources, Methodology, Investigation, Data curation, Conceptualization. **Daniela Montesarchio:** Writing – review & editing, Writing – original draft, Supervision, Resources, Methodology, Funding acquisition, Data curation, Conceptualization.

Declaration of competing interest

The authors declare the following financial interests/personal relationships which may be considered as potential competing interests: Daniela Montesarchio reports financial support was provided by Airc Italian Foundation for Cancer Research. Daniela Montesarchio reports financial support was provided by National Center for Gene Therapy and Drugs based on RNA Technology and the European Union-NextGeneration EU. If there are other authors, they declare that they have no known competing financial interests or personal relationships that could have appeared to influence the work reported in this paper.

Acknowledgements

The research leading to these results has received funding from: i) Fondazione AIRC under IG 2020—ID.25046 — P.I. Montesarchio Daniela; 2) CN00000041 National Center for Gene Therapy and Drugs based on RNA Technology and the European Union-NextGeneration EU – P.I. Montesarchio Daniela; iii) Federico II University, FRA2022 project (CUP: E65F22000050001) – P.I. Musumeci Domenica.

Appendix A. Supplementary data

Supplementary data to this article can be found online at https://doi.org/10.1016/j.ijbiomac.2025.148479.

Data availability

Data will be made available on request.

References

[1] C.K. Voong, J.A. Goodrich, J.F. Kugel, Interactions of HMGB proteins with the genome and the impact on disease, Biomolecules 11 (2021) 1451, https://doi.org/10.3390/biom11101451.
[2] D. Musumeci, G.N. Roviello, D. Montesarchio, R. Sapio, M. Valente, V. Anrò, E. M. Bucci, Hairpin ODN-based ligands as potential inhibitors of HMGB1 cytokine activity, RSC Adv. 3 (2013) 12176–12184, https://doi.org/10.1039/c3ra41915k.
[3] D. Musumeci, E.M. Bucci, G.N. Roviello, R. Sapio, M. Valente, M. Moccia, M. E. Bianchi, C. Pedone, DNA-based strategies for blocking HMGB1 cytokine activity: design, synthesis and preliminary in vitro/in vivo assays of DNA and DNA-like duplexes, Mol. Biosyst. 7 (2011) 1742–1752, https://doi.org/10.1039/c1mb05009e.
[4] Y. Jung, S.J. Lippard, Nature of full-length HMGB1 binding to cisplatin-modified DNA, Biochemistry 42 (2003) 2664–2671, https://doi.org/10.1021/bi026972w.
[5] M. Webb, J.O. Thomas, Structure-specific binding of the two tandem HMG boxes of HMG1 to four-way junction DNA is mediated by the A Domain, J. Mol. Biol. 294 (1999) 373–387, https://doi.org/10.1006/jmbi.1999.3150.
[6] R. Chen, R. Kang, D. Tang, The mechanism of HMGB1 secretion and release, Exp. Mol. Med. 54 (2022) 91–102, https://doi.org/10.1038/s12276-022-00736-w.
[7] D. Musumeci, G.N. Roviello, D. Montesarchio, An overview on HMGB1 inhibitors as potential therapeutic agents in HMGB1-related pathologies, Pharmacol. Ther. 141 (2014) 347–357, https://doi.org/10.1016/j.pharmthera.2013.11.001.
[8] J. Mo, J. Hu, X. Cheng, The role of high mobility group box 1 in neuroinflammatory related diseases, Biomed. Pharmacother. 161 (2023) 114541, https://doi.org/10.1016/j.biopha.2023.114541.
[9] S. Yuan, Z. Liu, Z. Xu, J. Liu, J. Zhang, High mobility group box 1 (HMGB1): a pivotal regulator of hematopoietic malignancies, J. Hematol. Oncol. 13 (2020) 1186, https://doi.org/10.1186/s13045-020-00920-3.
[10] T. Tamura, K. Kurishima, K. Nakazawa, K. Kagohashi, H. Ishikawa, H. Satoh, N. Hizawa, Specific organ metastases and survival in metastatic non-small-cell lung cancer, Mol. Clin. Oncol. 3 (2015) 217–221, https://doi.org/10.3892/mco.2014.410.
[11] H. Mithoowani, M. Febbraro, Non-small-cell lung cancer in 2022: a review for general practitioners in oncology, Curr. Oncol. 29 (2022) 1828–1839, https://doi.org/10.3390/curroncol29030150.
[12] N.A. Handke, A.B.A. Rupp, N. Trimpop, J. von Pawel, S. Holdenrieder, Soluble high mobility group box 1 (HMGB1) is a promising biomarker for prediction of therapy response and prognosis in advanced lung cancer patients, Diagnostics 11 (2021) 356, https://doi.org/10.3390/diagnostics11020356.
[13] S. Idoudi, T. Bedhiafi, S. Pedersen, M. Elahtem, I. Alremawi, S. Akhtar, S. Dermime, M. Merhi, S. Uddin, Role of HMGB1 and its associated signaling pathways in human malignancies, Cell. Signal. 112 (2023) 110904, https://doi.org/10.1016/j.cellsig.2023.110904.
[14] E. Napolitano, A. Criscuolo, C. Riccardi, C.L. Esposito, S. Catuogno, G. Coppola, G. N. Roviello, D. Montesarchio, D. Musumeci, Directing *in vitro* selection towards G-quadruplex-forming aptamers to inhibit HMGB1 pathological activity, Angew. Chem. Int. Ed. 63 (2024) e202319828, https://doi.org/10.1002/anie.202319828.
[15] E. Napolitano, A. Criscuolo, C. Riccardi, C. Platella, R. Gaglione, A. Arciello, D. Musumeci, D. Montesarchio, When annealing is detrimental: the case of HMGB1-targeting G-quadruplex aptamers, Int. J. Biol. Macromol. 283 (2024) 137148, https://doi.org/10.1016/j.ijbiomac.2024.137148.
[16] F. Moccia, C. Riccardi, D. Musumeci, S. Leone, R. Oliva, L. Petraccone, D. Montesarchio, Insights into the G-rich VEGF-binding aptamer V7t1: when two G-quadruplexes are better than one!, Nucleic Acids Res. 47 (2019) 8318–8331, https://doi.org/10.1093/nar/gkz589.
[17] C. Riccardi, E. Napolitano, D. Musumeci, D. Montesarchio, Dimeric and multimeric DNA aptamers for highly effective protein recognition, Molecules 25 (2020) 7–15, https://doi.org/10.3390/molecules25225227.
[18] Z. Wang, X. Yang, N.Z. Lee, X. Cao, Multivalent aptamer approach: designs, strategies, and applications, Micromachines (Basel) 13 (2022) mi13030436, https://doi.org/10.3390/mi13030436.
[19] Z. Moradi, K. Abnous, S.M. Taghdisi, J. Zamanian, M. Moshiri, D. Etemad, L. Etemad, P. Kesharwani, A. Sahebkar, Designing multivalent aptamers: recent advancements in diagnostic and therapeutic approaches for cancer treatment, J. Drug Deliv. Sci. Technol. 105 (2025) 106614, https://doi.org/10.1016/j.jddst.2025.106614.
[20] H. Hasegawa, K.-I. Taira, K. Sode, K. Ikebukuro, Improvement of aptamer affinity by dimerization, Sensors 8 (2008) 1090–1098, https://doi.org/10.3390/s8021090.
[21] K.M. Ahmad, Y. Xiao, H. Tom Soh, Selection is more intelligent than design: improving the affinity of a bivalent ligand through directed evolution, Nucleic Acids Res. 40 (2012) 11777–11783, https://doi.org/10.1093/nar/gks899.
[22] Y. Nonaka, W. Yoshida, K. Abe, S. Ferri, H. Schulze, T.T. Bachmann, K. Ikebukuro, Affinity improvement of a VEGF aptamer by in silico maturation for a sensitive VEGF-detection system, Anal. Chem. 85 (2013) 1132–1137, https://doi.org/10.1021/ac303023d.
[23] C. Riccardi, D. Musumeci, C. Platella, R. Gaglione, A. Arciello, D. Montesarchio, Tuning the polymorphism of the anti-VEGF G-rich V7t1 aptamer by covalent dimeric constructs, Int. J. Mol. Sci. 21 (2020) 1–24, https://doi.org/10.3390/ijms21061963.

[24] J.L. Mergny, Thermal difference spectra: a specific signature for nucleic acid structures, Nucleic Acids Res. 33 (2005) e138, https://doi.org/10.1093/nar/gni134.
[25] J.L. Mergny, L. Lacroix, UV melting of G-quadruplexes, Curr. Protoc. Nucleic Acid Chem. 37 (2009) 1–15, https://doi.org/10.1002/0471142700.nc1701s37.
[26] M. Małgowska, D. Gudanis, A. Teubert, G. Dominiak, Z. Gdaniec, How to study G-quadruplex structures, Biotechnologia 93 (2012) 381–390, https://doi.org/10.5114/bta.2012.46592.
[27] A.I. Karsisiotis, N.M.A. Hessari, E. Novellino, G.P. Spada, A. Randazzo, M. Webba Da Silva, Topological characterization of nucleic acid G-quadruplexes by UV absorption and circular dichroism, Angew. Chem. Int. Ed. 50 (2011) 10645–10648, https://doi.org/10.1002/anie.201105193.
[28] S. Masiero, R. Trotta, S. Pieraccini, S. De Tito, R. Perone, A. Randazzo, G.P. Spada, A non-empirical chromophoric interpretation of CD spectra of DNA G-quadruplex structures, Org. Biomol. Chem. 8 (2010) 2683–2692, https://doi.org/10.1039/c003428b.
[29] M. Vorlíčková, I. Kejnovská, J. Sagi, D. Renčiuk, K. Bednářová, J. Motlová, J. Kypr, Circular dichroism and guanine quadruplexes, Methods 57 (2012) 64–75, https://doi.org/10.1016/j.ymeth.2012.03.011.
[30] R. Del Villar-Guerra, R.D. Gray, J.B. Chaires, Characterization of quadruplex DNA structure by circular dichroism, Curr. Protoc. Nucleic Acid Chem. 2017 (2017) 17.8.1–17.8.16, https://doi.org/10.1002/cpnc.23.
[31] S. Paramasivan, I. Rujan, P.H. Bolton, Circular dichroism of quadruplex DNAs: applications to structure, cation effects and ligand binding, Methods 43 (2007) 324–331, https://doi.org/10.1016/j.ymeth.2007.02.009.
[32] R. del Villar-Guerra, J.O. Trent, J.B. Chaires, G-quadruplex secondary structure obtained from circular dichroism spectroscopy, Angew. Chem. Int. Ed. 57 (2018) 7171–7175, https://doi.org/10.1002/anie.201709184.
[33] P.A. Rachwal, K.R. Fox, Quadruplex melting, Methods 43 (2007) 291–301, https://doi.org/10.1016/j.ymeth.2007.05.004.
[34] M.M. Dailey, M. Clarke Miller, P.J. Bates, A.N. Lane, J.O. Trent, Resolution and characterization of the structural polymorphism of a single quadruplex-forming sequence, Nucleic Acids Res. 38 (2010) 4877–4888, https://doi.org/10.1093/nar/gkq166.
[35] E. Largy, J.L. Mergny, Shape matters: size-exclusion HPLC for the study of nucleic acid structural polymorphism, Nucleic Acids Res. 42 (2014) e149, https://doi.org/10.1093/nar/gku751.
[36] V. Rauser, E. Weinhold, Quantitative formation of monomeric G-quadruplex DNA from multimeric structures of c-Myc promoter sequence, ChemBioChem 21 (2020) 2445–2448, https://doi.org/10.1002/cbic.202000159.
[37] Y. Luo, A. Granzhan, J. Marquevielle, A. Cucchiarini, L. Lacroix, S. Amrane, D. Verga, J.L. Mergny, Guidelines for G-quadruplexes: I. In vitro characterization, Biochimie. 214 (2023) 5–23, https://doi.org/10.1016/j.biochi.2022.12.019.
[38] L. Petraccone, N.C. Garbett, J.B. Chaires, J.O. Trent, An integrated molecular dynamics (MD) and experimental study of higher order human telomeric quadruplexes, Biopolymers 93 (2010) 533–548, https://doi.org/10.1002/bip.21392.
[39] L. Petraccone, C. Spink, J.O. Trent, N.C. Garbett, C.S. Mekmaysy, C. Giancola, J. B. Chaires, Structure and stability of higher-order human telomeric quadruplexes, J. Am. Chem. Soc. 133 (2011) 20951–20961, https://doi.org/10.1021/ja209192a.
[40] J.K. Barrows, M.W. Van Dyke, Biolayer interferometry for DNA-protein interactions, PloS One 17 (2022) e0263322, https://doi.org/10.1371/journal.pone.0263322.
[41] K. Sathiyamoorthy, J. Jiang, Y.X. Hu, C.L. Rowe, B.S. Möhl, J. Chen, W. Jiang, E. D. Mellins, R. Longnecker, Z.H. Zhou, T.S. Jardetzky, Assembly and architecture of the EBV B cell entry triggering complex, PLoS Pathog. 10 (2014) e1004309, https://doi.org/10.1371/journal.ppat.1004309.
[42] X.H. Wang, S.Y. Zhang, M. Shi, X.P. Xu, HMGB1 promotes the proliferation and metastasis of lung cancer by activating the Wnt/β-catenin pathway, Technol. Cancer Res. Treat. 19 (2020) 1–8, https://doi.org/10.1177/1533033820948054.
[43] R. Palumbo, M. Sampaolesi, F. De Marchis, R. Tonlorenzi, S. Colombetti, A. Mondino, G. Cossu, M.E. Bianchi, Extracellular HMGB1, a signal of tissue damage, induces mesoangioblast migration and proliferation, J. Cell Biol. 164 (2004) 441–449, https://doi.org/10.1083/jcb.200304135.
[44] L. Zhu, S. Ren, M.J. Daniels, W. Qiu, L. Song, T. You, D. Wang, Z. Wang, Exogenous HMGB1 promotes the proliferation and metastasis of pancreatic cancer cells, Front. Med. (Lausanne) 8 (2021) 756988, https://doi.org/10.3389/fmed.2021.756988.
[45] J. Amato, L. Cerofolini, D. Brancaccio, S. Giuntini, N. Iaccarino, P. Zizza, S. Iachettini, A. Biroccio, E. Novellino, A. Rosato, M. Fragai, C. Luchinat, A. Randazzo, B. Pagano, Insights into telomeric G-quadruplex DNA recognition by HMGB1 protein, Nucleic Acids Res. 47 (2019) 9950–9966, https://doi.org/10.1093/nar/gkz727.
[46] K.P. de Carvasal, C. Riccardi, I.R. Krauss, D. Cavasso, J.J. Vasseur, M. Smietana, F. Morvan, D. Montesarchio, Charge-transfer interactions stabilize g-quadruplex-forming thrombin binding aptamers and can improve their anticoagulant activity, Int. J. Mol. Sci. 22 (2021) 9510, https://doi.org/10.3390/ijms22179510.
[47] L. Mollica, F. De Marchis, A. Spitaleri, C. Dallacosta, D. Pennacchini, M. Zamai, A. Agresti, L. Trisciuoglio, G. Musco, M.E. Bianchi, Glycyrrhizin binds to high-mobility group box 1 protein and inhibits its cytokine activities, Chem. Biol. 14 (2007) 431–441, https://doi.org/10.1016/j.chembiol.2007.03.007.
[48] W.A. Kibbe, OligoCalc: an online oligonucleotide properties calculator, Nucleic Acids Res. 35 (2007) 43–46, https://doi.org/10.1093/nar/gkm234.
[49] E. Napolitano, C. Riccardi, R. Gaglione, A. Arciello, V. Pirota, A. Triveri, F. Doria, D. Musumeci, D. Montesarchio, Selective light-up of dimeric G-quadruplex forming aptamers for efficient VEGF165 detection, Int. J. Biol. Macromol. 224 (2023) 344–357, https://doi.org/10.1016/j.ijbiomac.2022.10.128.
[50] V. Roviello, D. Musumeci, A. Mokhir, G.N. Roviello, Evidence of Protein Binding by a Nucleopeptide Based on a Thyminedecorated L-Diaminopropanoic Acid through CD and In Silico Studies, Curr Med Chem 28 (24) (2021) 5004–5015, https://doi.org/10.2174/0929867328666210201152326.
[51] C. Riccardi, K. Pérez de Carvasal, C. Platella, A. Meyer, M. Smietana, F. Morvan, D. Montesarchio, Probing naphthalene diimide and 3-hydroxypropylphosphate as end-conjugating moieties for improved thrombin binding aptamers: structural and biological effects, Bioorg. Chem. 141 (2023) 106917, https://doi.org/10.1016/j.bioorg.2023.106917.